

On the Prediction of Spray A End of Injection Phenomenon Using Conditional Source-term Estimation

X.H. Fang, R. Ismail, N. Sekularac and M. H. Davy

Department of Engineering Science, University of Oxford, UK

Abstract

In this study, the role of turbulence-chemistry interaction in diesel spray auto-ignition, flame stabilization and end of injection phenomena is investigated under engine relevant “Spray A” conditions. A recently developed diesel spray combustion modelling approach, Conditional Source-term Estimation (CSE-FGM), is coupled with Reynolds-averaged Navier-Stokes simulation (RANS) framework to study the details of spray combustion. The detailed chemistry mechanism is included through the Flamelet Generated Manifold (FGM) method. Both unsteady and steady flamelet solutions are included in the manifold to account for the auto-ignition process and the subsequent flame propagation in a diesel spray. Conditionally averaged chemical source terms are closed by the conditional scalars obtained in the CSE routine. Both non-reacting and reacting spray jets are computed over a wide range of Engine Combustion Network (ECN) diesel “Spray A” conditions. The reacting spray results are compared with simulations using a homogeneous reactor combustion model and a flamelet combustion model with the same chemical mechanism. The present study represents the first application of CSE for a diesel spray. The non-reacting liquid/vapour penetration, the mean and rms mixture fraction, the reactive region, the flame lift-off and the ignition delay show a good agreement with literature data from an optically accessible combustion vessel over a wide range of tested conditions. The CSE-FGM model also shows a better capability in predicting the end-of-injection events in diesel spray combustion. Overall, the CSE-FGM model is shown to capture the experimental trends well, both quantitatively and qualitatively.

Introduction

Modern compression ignition engines are designed to have fuel lean and low temperature combustion (LTC), therefore reducing emissions [20]. Under these conditions, mixing, chemical kinetics and turbulence-chemistry interactions play a significant role in the prediction of diesel spray flame characteristics such as, autoignition, flame lift-off and flame stabilization. While a number of studies have explored the fundamentals of auto-ignition and flame stabilization mechanisms at low temperature conditions [29][18], only a limited of studies have focused on the turbulence chemistry interactions at the end of injection (EOI). Previous studies have shown that the end of

injection processes can enhance ambient gas entrainment therefore affecting the hydrocarbon emissions [17]. One of the EOI processes, combustion recession, has been found in experiments to promote flame recession at the end of injection towards the injector tip thereby consuming some of the excess unburned hydrocarbons often associated with low-temperature combustion regimes [16]. A schematic of combustion recession for a typical non-premixed lifted flame can be found in Figure 1.

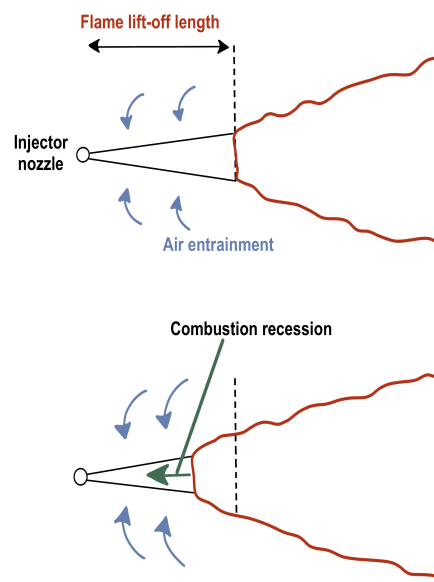


Figure 1. Schematic of combustion recession, adapted from [16].

Although many experiments have shown the existence and characteristics of combustion recession, there are relatively fewer simulation studies of the phenomenon - perhaps due to its transient nature. The high temperature ignition front of combustion recession was seen in experiments to “propagate” back towards the injector tip in the form of separate high temperature pockets where the speed of the “propagation” exceeded any physically reasonable flame speed [26]. Combustion recession, therefore, is perceived as a series of auto-ignition events as opposed to flame propagation back to the nozzle. The presence of repeated ignition and reignition

events during the combustion recession process has made its numerical simulation a challenging problem for the modelling community. Knox *et al.* [16] successfully interpreted the experimental trends, however the model was not capable of providing qualitative comparison between the simulation and the experiment. Kim *et al.* [15] and Jarrahbashi *et al.* [13] compared the efficacy of Well-Stirred Reactor (WSR) and Representative Interactive Flamelets (RIF) models in predicting flame initial stabilization characteristics and combustion recession, showing in the process that the choice of combustion model plays a significant role in the ability to predict combustion recession. The inclusion of turbulent mixing in the RIF model significantly changed the turbulent mean scalar fields, which may then better represent unsteady flame flapping motions. In the authors' previous work, an unsteady Flamelet Generated Manifold (FGM) combustion model was implemented to study the influence of turbulent chemistry interaction on combustion recession [8]. Further studies on chemical mechanisms [7] showed that low-temperature chemistry is a driving force for second-stage ignition in diesel spray end-of-injection processes. Although these studies showed good agreement with the experiment in terms of predicting flame initial stabilization and the occurrence of combustion recession under different ambient conditions, the true physical nature of combustion recession, as being the observed result of a series of ignition pockets, was not captured. In a study of diesel spray split injections, Blomberg *et al.* [3] explored combustion recession in both RANS and LES frameworks using a Conditional Moment Closure (CMC) combustion model which showed promising potential for modelling spray transient phenomenon. Although RANS-CMC did not capture full combustion recession towards upstream nozzle location after first injection, the evidence of separate ignition pockets after end of first injection moving towards the injector tip was clearly visible in the LES-CMC simulations.

In this study, a novel combustion modelling approach, CSE-FGM, is applied to study the Engine Combustion Network (ECN) diesel "Spray A". First, the efficacy of the CSE-FGM model is explored with respect to the "Spray A" autoignition and flame development characteristics for the baseline conditions and also for parametric variations of ambient temperature and oxygen concentration. The modelling results are compared with the available experimental data and previous simulations performed using well-stirred reactor (SAGE) model. This includes a detailed description of the trends followed by the ignition delay, the flame lift-off length, and the analysis of flame spatial contours. The auto-ignition process and the reacting spray structure are also discussed in detail. Finally, the prediction of the combustion recession using the CSE-FGM model is examined. The flame structure is analyzed in detail compared to earlier simulations using different combustion models.

Computational Set-up

The entire modelling routine is developed in the commercially available CFD solver CONVERGE through user-defined functions. The Pressure Implicit with Splitting of Operators (PISO) [12] was used to solve the transport equations. All

transported variables in CONVERGE are co-located at the centre of the cell. The Rhie-Chow [27] algorithm was used to prevent checker-boarding. Second-order accurate central differencing schemes were used for spatial discretization in all simulations, with fully implicit first-order accurate time integration to maintain stability. A variable time-step was used based on the Courant-Friedrichs-Lewy (CFL) condition for convection ($CFL_u = u \frac{\Delta t}{\Delta x}$), diffusion ($CFL_v = v \frac{\Delta t}{\Delta x^2}$) and speed of sound ($CFL_c = c \frac{\Delta t}{\Delta x}$). Here, Δx is the grid size, Δt is the time-step, u is the cell velocity, v is the dynamic viscosity and c is the speed of sound. The capability of the CSE model is primarily validated against the ECN "Spray A" baseline conditions listed in Table 1 (Test II) using RANS turbulence closure. Turbulence was modelled using the RANS $k-\epsilon$ model with modified model constants given in authors previous study [8]. Variations of the ambient temperature and the oxygen concentration were simulated in this study to assess the performance of CSE and the effect of ambient conditions on end of injection phenomenon, combustion recession. All test conditions performed in this study are summarized in Table 1. The well known Lagrangian-Eulerian framework was used to model the liquid phase where all sub-models used are stated in Table 3. More detailed spray modelling set-up and sub-model constants can be found in the group's previous publications [8][7]. The chemical mechanism chosen for this study is the 54 species, 268 reactions Yao *et al.* [30] mechanism (later referred to as the Yao mechanism). The computational domain is set to be volumetrically identical to the experimental combustion vessel at the Sandia National Laboratories [26]. A systematic mesh resolution and grid sensitivity study was previously conducted by the authors [8]. For this study, adaptive mesh refinement (AMR) is used allowing the base volume of a computational cell to be split into smaller volume during run time. Based on previous study, the base grid of this particular case is chosen as 2 mm and the smallest grid scale allows via 3 levels of AMR corresponding to 0.25 mm. A near nozzle section view of the computational domain can be seen in Figure 2. For the present studies, all simulations are performed locally on workstations with 20 cores at 2.4~2.5 GHz of clock speed and 64 GB of RAM size.

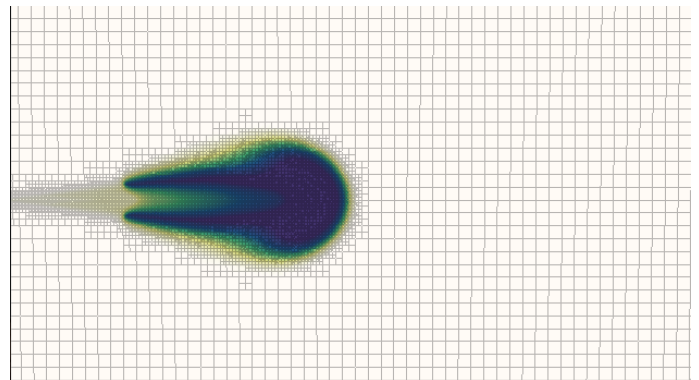


Figure 2. Computational domain showing AMR.

Table 1. ECN Sandia “Spray A” experimental nominal test conditions [25]. Test II denotes ECN “baseline” dition.

Test	O ₂ [% volume]	T _{amb} [K]	Unchanged
0	0	900	Fuel = NC12H26
I	15	800	Fuel mass = 14 [mg]
II	15	900	$\phi_{nozzle} = 0.090$ [mm]
III	15	1100	$\rho_{amb} = 22.8$ [kgm ⁻³]
IV	13	900	T _{fu} = 363 [K]
V	21	900	P _{inj} 150 [MPa]

Table 2. ECN Sandia “Spray A” combustion vessel initial species mole fractions [25].

O ₂	N ₂	CO ₂	H ₂ O
00.00	89.71	06.52	03.77
15.00	75.15	06.23	03.62

Combustion Model

Conditional Source-term Estimation, or more commonly CSE, was firstly proposed by Bushe and Steiner [1]. Following the same first order hypothesis as CMC for closing chemical source terms and therefore neglecting the conditional fluctuations, the mean conditional chemical source term for species k is defined as follows:

$$\overline{\omega_k|\eta} \approx \omega_k(\overline{T|\eta}, \overline{Y_k|\eta}, \overline{\rho|\eta}) \quad (1)$$

where η is a conditioning variable, $\overline{T|\eta}$ is the conditional temperature, $\overline{Y_k|\eta}$ and $\overline{\rho|\eta}$ are respectively the conditional mass fraction of species k and density. Keep in mind that for combustion processes occurring in diffusion flames, η is chosen as the mixture fraction, Z . The unconditional mean chemical source term is obtained by integrating the conditional value mentioned above (Equation 1) over the PDF of η defined below as:

$$\overline{\omega_k}(\vec{x}, t) = \int_0^1 \overline{\omega_k|\eta}(\eta, \vec{x}, t) \tilde{P}(\eta, \vec{x}, t) d\eta \quad (2)$$

such that $\tilde{P}(\eta, \vec{x}, t)$ is the Favre averaged PDF of the mixture fraction usually defined through a β -function [9]. The conventional CMC approach (a typical CMC solving process can be found in Figure 3) is based on solving transport equations for conditional mass fractions. Such transport equations contain several unclosed terms that then require substantially greater computational time to solve compared to the CSE approach. Closure of these terms are a modelling challenge especially in premixed flames [21]. In CSE (a conventional CSE solving process for a methane-air flame can be seen in Figure 4), the conditionally averaged scalars are obtained by inverting the following integral equation (a Fredholm integral equation of the first kind):

$$\tilde{Y}_k(\vec{x}, t) = \int_0^1 \overline{Y_k|\eta}(\eta, \vec{x}, t) \tilde{P}(\eta, \vec{x}, t) d\eta \quad (3)$$

where \vec{x} , t and \tilde{Y}_k are respectively the spatial coordinate, time and the fluctuation of the mass fraction of the k^{th} chemical

Table 3. Spray simulation discrete phase sub-models.

Sub-models	
Injection	Blob method
Droplet breakup	KH-RT without breakup length
Droplet drag	Dynamic droplet drag
Droplet collisions	No Time Counter
Vaporisation	Frossling correlation
Droplet heat transfer	Ranz-Marshall
Turbulent dispersion	O’Rourke

species defined as $\tilde{Y}_k \equiv \overline{Y_k}/\overline{\rho}$. CSE makes the assumption of spatial homogeneity for conditional means [1] also commonly taken in the CMC combustion model to reduce the computational cost of the simulation [21]. Hence, localized cells referred to as an ensemble, may be selected in the flow field with statistical homogeneity in conditional averages enabling Equation 3 to be rewritten as below:

$$\tilde{Y}_k(\vec{x}_j, t) = \int_0^1 \overline{Y_k|\eta}(\eta, \vec{x}_j, t) \tilde{P}(\eta, \vec{x}_j, t) d\eta \quad x_j \in D \quad (4)$$

where x_j is the spatial coordinate of the j^{th} point in the ensemble D . $\tilde{Y}_k(\vec{x}_j, t)$ in the above equation are determined via transport equations while $\overline{Y_k|\eta}(\eta, \vec{x}_j, t)$ are the unknown values of this problem. This equation must be solved at every time step in the reacting flow solver to provide the conditional averages enabling Equation 1 to close the chemical reaction source terms. As mentioned previously, Equation 4 is a Fredholm integral equation with $\tilde{P}(\eta, \vec{x}_j, t)$ as the kernel [19]. Hence, it can be rewritten in a numerical expression i.e. discrete form defined below as:

$$\vec{b} = \mathbf{A} \vec{\alpha} \quad (5)$$

where \vec{b} is the unconditional Favre average mass fraction of species k at \vec{x}_j position i.e. $\tilde{Y}_k(\vec{x}_j, t)$ while $\vec{\alpha}$ is the conditional mean in the i^{th} bin i.e. $\overline{Y_k|\eta}(\eta, \vec{x}_j, t)$. On the other hand, \mathbf{A} is an $N \times M$ matrix with $N > M$ of the integrated PDF over some interval of the mixture fraction, where N is the number of points in each ensemble and M being the number of bins in mixture fraction space. \mathbf{A} can be computed as:

$$A_{ji} = \int_{\eta_1}^{\eta_2} \tilde{P}(\eta_i, \vec{x}_j, t) d\eta \quad (6)$$

The solution of Equation 5 i.e. $\vec{\alpha} = \mathbf{A}^{-1} \vec{b}$, is sensitive to any perturbations in the system which makes it an ill-posed problem [11]. Different methods exist nowadays enabling solving this issue. Bushe and Steiner [1] introduced an approach minimizing the residual of Equation 4 and the conditional averages’ derivatives with respect to mixture fractions. Tikhonov proposed a regularisation approach based on an *a priori* knowledge of the solution later introduced by Grout *et al.* [10]. One way to implement this approach is to solve the following least-squares problem to obtain the solution of Equation 5:

$$\tilde{\alpha} = \underset{\alpha}{\operatorname{argmin}} \left\| \begin{bmatrix} A \\ \lambda I \end{bmatrix} \tilde{\alpha} - \begin{bmatrix} \vec{b} \\ \lambda \tilde{\alpha}^0 \end{bmatrix} \right\|_2^2, \quad (7)$$

where $\|\cdot\|_2$ denotes the L2 norm of a vector, I is the identity matrix, λ is the regularization parameter and $\tilde{\alpha}^0$ is the prior knowledge of solution which may take any initial value as the solution will be independent of this. Keep in mind that λ is evaluated based on the characteristics of the inversion problem and according to [10] can be defined as follows:

$$\lambda = \frac{\operatorname{Tr}(A^T A)}{I} \quad (8)$$

where Tr is the trace of the matrix. As mentioned earlier, CSE is more computationally attractive than CMC and just like the Doubly Conditional Moment Closure (DCMC), the Doubly Conditional Source-term Estimation (DCSE) can also be used for simulating combustion phenomena such as extinction and reignition. Indeed, Dovizio *et al.* [5][4] managed successfully to predict these phenomena in both turbulent stratified V-shaped flames and a series of lifted turbulent jet flames. Incorporating detailed chemistry, whether it is in CMC or CSE, is a challenging task particularly for ‘real’ hydrocarbon fuels. These are characterised by hundreds of species and thousands of reactions – each requiring the solution of the related transport equations – therefore increasing drastically computational time. Hence, a reduced chemistry model is mandatory so that a limited number of scalars can represent the detailed chemistry. Previous CSE studies focussed on low carbon fuels where Trajectory Generated Low-dimensional Manifolds (TGLDM) were found to be suitable for chemistry reduction. However, further studies have shown that the conventional TGLDM might not be suitable for diesel surrogate. Therefore, within the framework of this paper, a Flamelet Generated Manifold has been established enabling a more sophisticated chemistry reduction mechanism.

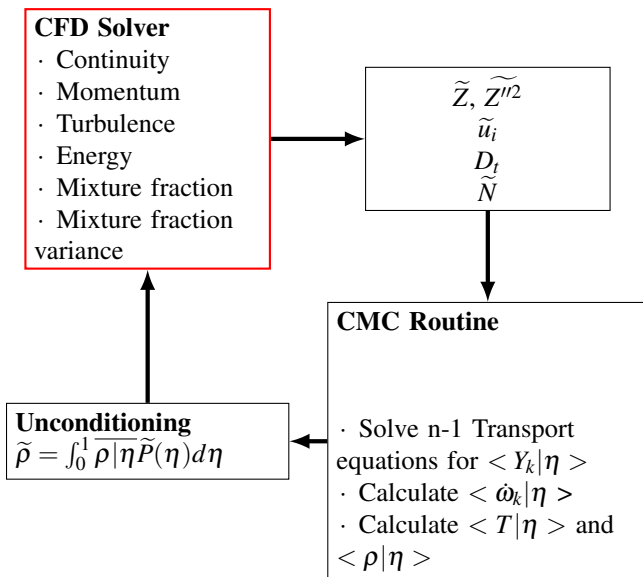


Figure 3. Typical CMC routine structure

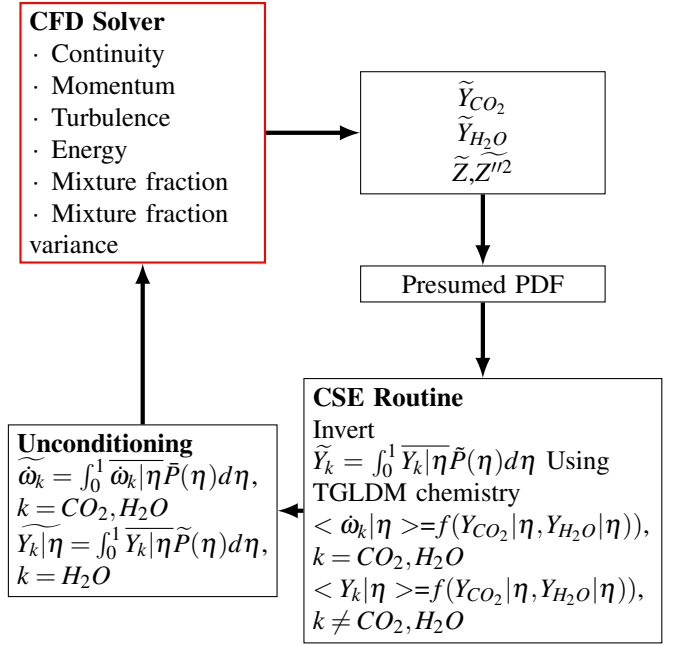


Figure 4. CSE routine structure for a typical methane-air flame

Flamelet Generated Manifold

In the present work, chemistry tabulation is based on the Flamelet Generated Manifold (FGM) approach where one-dimensional flamelet solutions are pre-computed using detailed chemistry and parametrized using a reduced number of control variables.

Canonical flame configuration

Depending on the combustion application, a flame configuration must be selected that adequately represents the chemical processes taking place in the flame of interest. Diesel combustion is predominantly non-premixed and is therefore best represented by the igniting counter-flow diffusion flame (ICDF). In this flame, oxidizer and fuel streams are opposed to each other forming a reaction zone perpendicular to the streams as illustrated in Figure 5. Straining of the flame is achieved by either increasing the flow velocities or reducing the distance between the two streams. An unstrained flame will depart from chemical equilibrium with increasing strain up until it quenches.

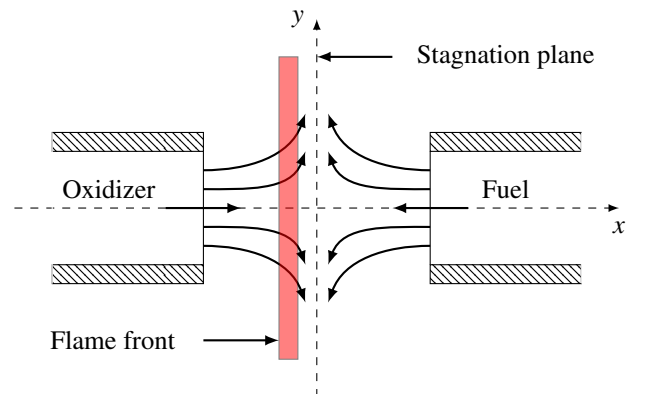


Figure 5. Schematic of laminar non-premixed counterflow diffusion flame

Following Stahl & Warnatz [28] the one-dimensional governing equations for an ICDF are given as:

$$\frac{\partial \rho}{\partial t} + \frac{\partial}{\partial x}(\rho u) = -\rho K \quad (9)$$

$$\frac{\partial \rho Y_i}{\partial t} + \frac{\partial \rho u Y_i}{\partial x} = \frac{\partial}{\partial x} \left(\rho D \frac{\partial Y_i}{\partial x} \right) + \dot{\omega}_i - \rho K Y_i \quad (10)$$

$$\frac{\partial \rho h}{\partial t} + \frac{\partial \rho u h}{\partial x} = \frac{\partial}{\partial x} \left(\frac{\lambda}{c_p} \frac{\partial h}{\partial x} \right) - \rho K h \quad (11)$$

$$\rho \frac{\partial K}{\partial t} + \rho u \frac{\partial K}{\partial x} = \frac{\partial}{\partial x} \left(\mu \frac{\partial K}{\partial x} \right) + \rho_{ox} a^2 - \rho K^2 \quad (12)$$

where $K(x, t) = \frac{\partial u_y}{\partial y}$, is the strain rate or flame stretch field, which is a function of the x coordinate and the applied strain rate a at the oxidizer boundary. D is the diffusion coefficient defined as $D = \frac{\lambda}{\rho c_p}$. For non-premixed flames a unity Lewis number is assumed in order to simplify the transport equations. In this work the CHEM1D code of Eindhoven University of Technology is used to solve one-dimensional ICDF in physical space and time with detailed chemistry. Figure 6 illustrates temperature evolution as a function of spatial coordinate x and time for a laminar counter-flow diffusion flame at engine-like conditions. N-dodecane fuel flows in from the right and oxidizer diluted with EGR flows in from the left at a strain rate of 500 s^{-1} . A purely mixing solution (frozen chemistry) at the test conditions (temperature, pressure, species mass fraction and strain rate) is used as initialisation to the ICDF as indicated by the black line. The ignition process is then tracked from this mixing solution in time (blue lines) until a quasi steady state flame is reached (red line).

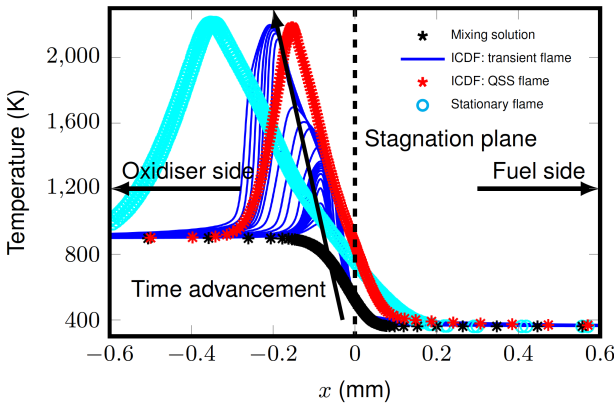


Figure 6. Temperature evolution $T(x, t)$ of flamelet solutions obtained for 900 K reacting ‘‘Spray A’’ baseline conditions of a counter flow diffusion flame.

Parametrization of FGM

The full composition space of the flamelet solutions is described by $N_s + 2$ -dimensional solutions spanned by enthalpy, pressure and N_s number of species. Through careful consideration, a reduced set (any number or combination) of controlling variables can be used to parametrize the flamelet solutions as long as the full mixture composition is described. Increasing

the number of controlling variables will increase accuracy up to $N_s + 2$ dimensions, where eventually the full composition space will be recovered. As this work will focus on spray combustion applications: fuel-oxidizer mixing, ignition and combustion progression in the diffusion flame are the main physical phenomena of interest. Mixing can be described by the mixture fraction, Z using the definition of Bilger [2]. The mixture fraction is a monotonic function of spatial coordinate x which allows direct mapping of flamelet solutions from physical space to mixture fraction space as shown in Figure 7. Starting from the mixing solution up until chemical equilibrium, any variable that continuously increases or decreases with time can be used to describe ignition and combustion progression. In this work, the reaction progress variable c , is defined as weighted linear combination of certain key species mass fractions that represent each stage of combustion evolution:

$$c = \frac{Y_{\text{CH}_2\text{O}}}{Y_{\text{CH}_2\text{O}}^{eq}} + \frac{Y_{\text{CO}}}{Y_{\text{CO}}^{eq}} + \frac{Y_{\text{CO}_2}}{Y_{\text{CO}_2}^{eq}} \quad (13)$$

To capture ignition, formaldehyde (CH_2O) is included as it is found in high concentrations at the onset of ignition [29]. Major combustion products of CO and CO_2 represent the intermediate and end phases of combustion. In order for each species in the reaction progress variable definition to have a balanced contribution, it is weighted by its equilibrium mass fraction.

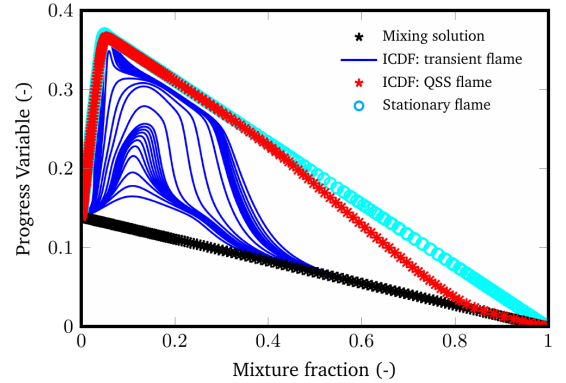


Figure 7. Flamelet solutions in progress variable-mixture fraction space for a counter flow diffusion flame. Black line represents a mixing solution; blue lines represent time-sampled transient flamelet solutions, red symbols denote a quasi-steady state flame and the teal symbols show the steady flamelet solution.

To account for combustion in a steady flame, the FGM database generated by ICDFs is extended further by including solutions of steady flamelets at strain rates varying from the highest non-quenching strain rate down to $a = 1 \text{ s}^{-1}$. This covers the entire Z - c space from the mixing line up to chemical equilibrium. The resultant manifold is shown in Figure 8. All flamelet calculations are carried out assuming constant pressure and conserved enthalpy, therefore, if variations in any of these quantities occur, additional dimensions will be required in the FGM database in order to account for the influence of these variables on combustion. The entire solving process of the currently implemented CSE-FGM combustion model can be seen in Figure 9. It is worth noting that for each of the conditions tested, a corresponding manifold is needed for the calculation of CSE.

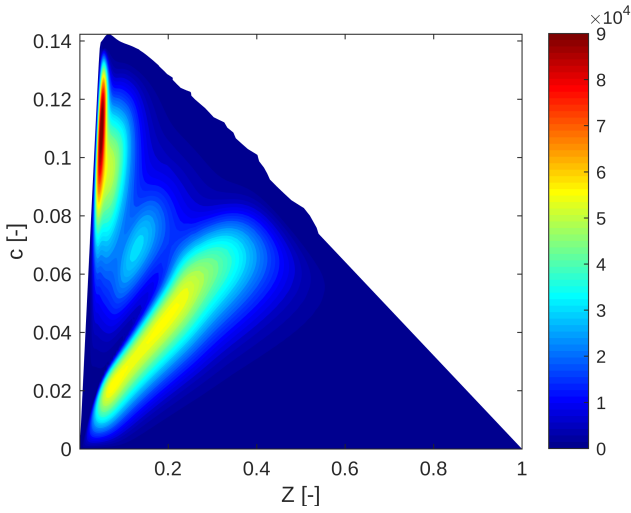


Figure 8. Example of a flamelet generated manifold showing reaction rate of c as a function of mixture fraction and progress variable at 900 K “Spray A” baseline conditions

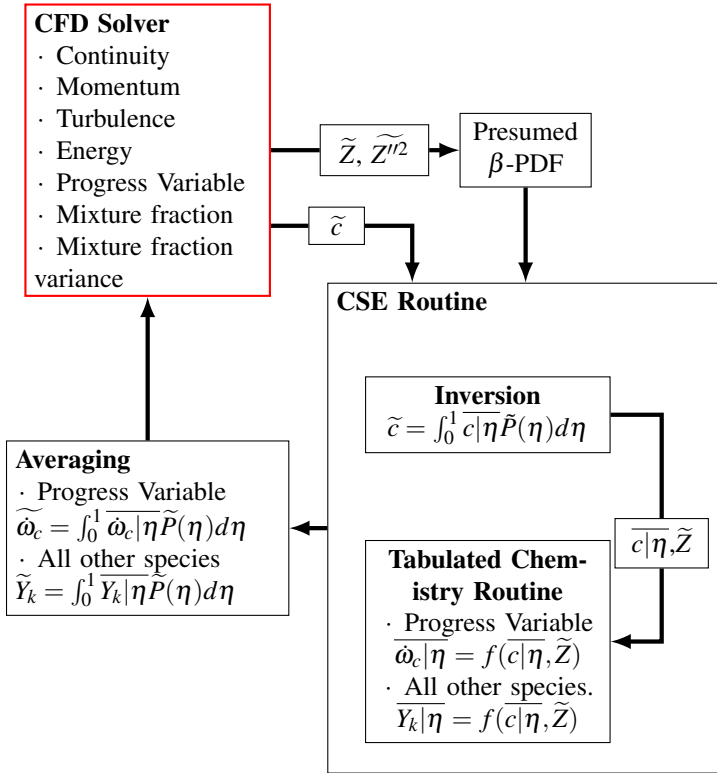


Figure 9. CSE Routine Structure for ECN diesel “Spray A”

Non-reacting spray results

In order to have an accurate reacting spray case, a non-reacting spray is first modelled and compared with the experiment. The test conditions for the non-reacting spray study are listed in Table 1 as Test 0. Liquid penetration, vapour penetration and mixture fraction profiles are validated against the experiment. In this study liquid penetration is defined as the axial location of 95% liquid mass threshold. And the vapour penetration is defined as the maximum distance from the injector to where the fuel mass fraction is 0.1%. Figure 10 shows the liquid and vapour penetration length between the simulation and the

experiment. The predictions for both criteria are in excellent agreement with the experimental measurements. Furthermore radial mixture fraction profiles at two axial downstream locations are shown in Figure 11. Slight underprediction is found near the center of the liquid jet. This is likely due to the size of computational grid bigger than the spray droplet size. However, further downstream on the axial direction and the outer periphery of the spray in radial direction showed good agreement with the experiment.

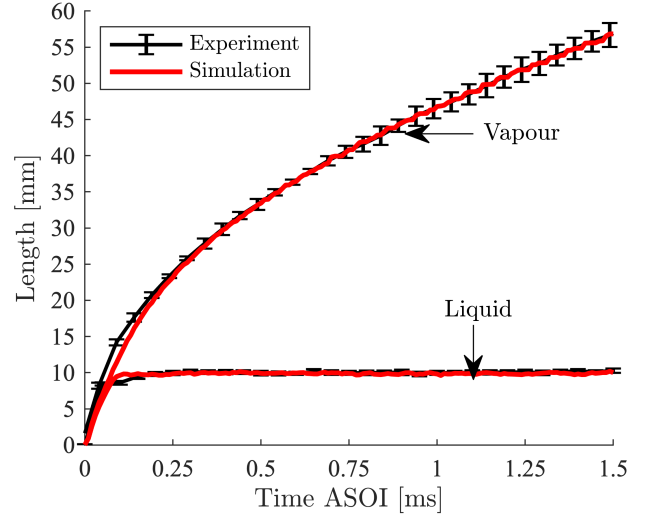


Figure 10. Non-reacting liquid and vapor penetration for “Spray A” baseline conditions

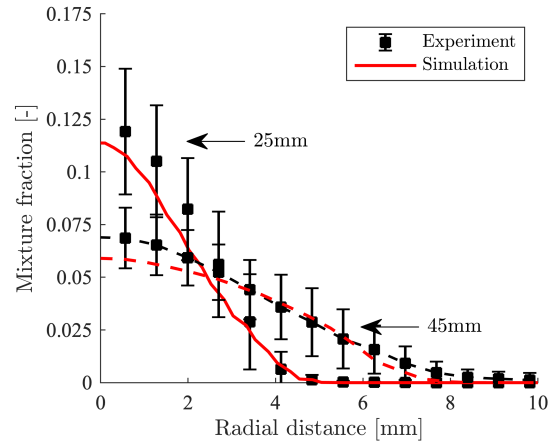


Figure 11. Mixture fraction radial profile for non-reacting “Spray A” baseline case at two axial downstream locations

Reacting Spray Results

The validity of the implemented CSE-FGM combustion model is first tested across a wide range of ambient conditions. The results are compared with the current CONVERGE well stirred reactor (SAGE) combustion model as well as the experimental data. Both the ignition delay time and the lift-off length predictions for all conditions tested are presented in Figure 12, Figure 13, Figure 16 and Figure 17. The definition of the IDT

and LOL follows the ECN simulation guidelines where the IDT is defined as the first time at which Favre averaged OH mass fraction reaches 2% of the domain maximum after steady state is established. The LOL is defined as the distance from the injector to the first location where the Favre averaged OH mass fraction reaches 14% of the instantaneous maximum during the steady state period. For the temperature and oxygen concentration sweep, the CONVERGE well-stirred reactor combustion model is applied to the same conditions listed in Table 1 and then compared to the CSE-FGM result. Figure 12 showed both combustion models can accurately predict the trend of ignition delay under different ambient temperature conditions where ignition is prolonged when ambient temperature is lower. Similar trends for flame lift-off length under various ambient temperature is also predicted by the two combustion models (shown in Figure 13). An overprediction in both the IDT and the LOL is seen for WSR combustion model with more visible discrepancy observed at lower ambient temperature. Previous studies have found the inclusion of turbulent chemistry interaction and sub-grid variance plays an important role at low temperature ignition [18][24]. With the current CSE routine including both of these terms, both first and second stage ignition can be more accurately captured under low-temperature conditions. A more detailed ignition behaviour study was conducted through the analysis of temperature - mixture fraction scatter plot and the comparison of experimental schlieren image and temperature contour at “Spray A” baseline conditions.

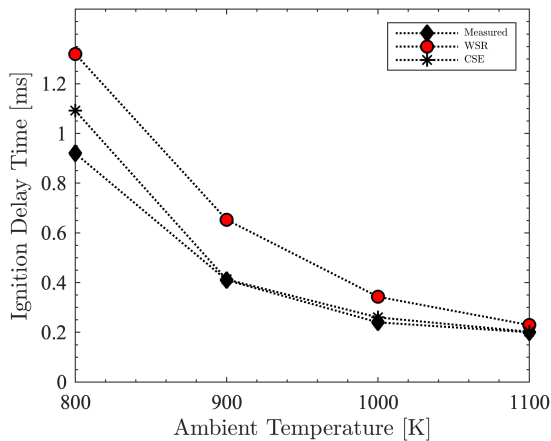


Figure 12. Simulation and experimental ignition delay timings for different “Spray A” ambient temperature conditions

Figure 14 shows the temporal evolution scatter plot of temperature in mixture fraction space around ignition delay time. At 0.19 ms, all the points are clustered around the mixing line. Low temperature reactions have been initiated at the edge of spray jet. These reactions first occur in leaner mixtures as these are at the highest temperature in the unburnt flow field. Prior to second stage combustion at around 0.40 ms, most points in the figure are clustered in the rich mixture zone. The low temperature reactions, predominantly initiated by the first-stage ignition, here coupled with the high scalar dissipation rate in this region, initiate a turbulent cool-flame which transports species and heat release to colder and richer mixtures. This is demonstrated by the shift in conditional temperature, from leaner to richer mixtures. It is worth noting

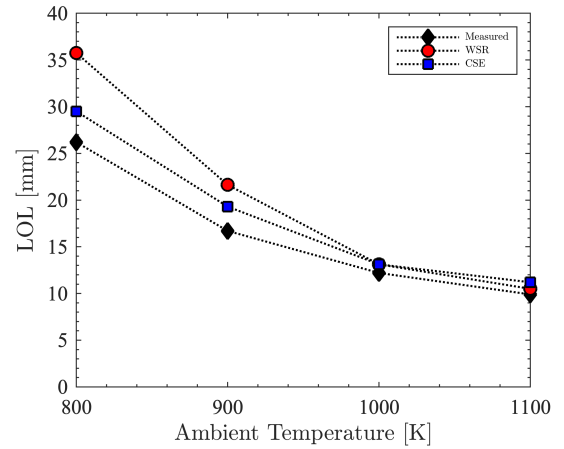


Figure 13. Simulation and experimental lift-off length for different “Spray A” for different ambient temperature conditions

that the current study gives a smooth transition of temperature at different mixture fractions. This is likely due to the “ensemble averaging” process in RANS smoothing out this apparent abrupt transition. At second stage combustion, the combustion event is favouring a mixture fraction of less than 0.15. The temperature continues to rise and the mean temperature becomes closer to the equilibrium state. At 0.45 ms the highly stratified flow field, formed from high temperature ignition, initiates turbulent flame propagation from richer to leaner mixtures.

Due to the challenging operating conditions of diesel combustion, limited experimental data is available for model validation. Various diagnostic techniques have been used in different institutions, such as high-speed schlieren, Mie-scattering and chemiluminescence imaging. However despite substantial coordinated efforts within the ECN community, only partial sets of data are provided, typically with only one or two species available simultaneously. Quantitative experimental measurements of local mixture-fraction, species mass fractions, velocity field and temperature field are not yet available for reacting conditions. Therefore only qualitative comparisons can be made at this time between the experimental data and the simulation. In order to further study the ignition prediction and the following flame temporal evolution for the current combustion model, Figure 15 shows comparisons between the simulations and the experimental schlieren images for the 900 K “Spray A” baseline conditions. To aid the visualization of the high temperature reaction, the border of the high-temperature chemiluminescence (blue line) is overlaid on the simultaneously-acquired schlieren images. The details of image processing and experimental set up can be found in [26]. The ignition delay to high temperature combustion in the experiment is marked by the first combustion luminosity, which appears around 410 μ s ASI. The simulation accurately predicted the ignition event. Second stage ignition region is well matched between the experiments and the simulations. For the flame evolution, even if a quantitative assessment is not possible, the computed distributions from simulation shows a good agreement throughout the evolution of the flame. The high temperature luminosity line of the experiment is located at the edge of the flame where high temperature reactions exist. In

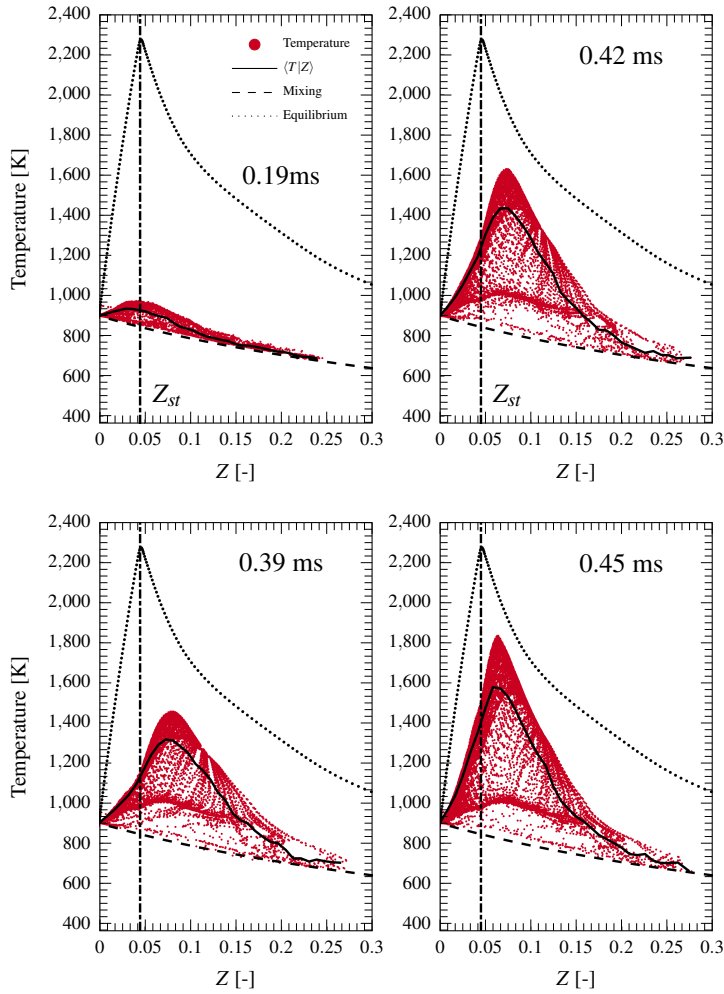


Figure 14. Temporal evolution of scatter plot of temperature versus mixture fraction for the 900K “Spray A” baseline conditions.

contrast, the simulation moves the Z_{st} line to the center of the flame. This is likely due to RANS being an ensemble averaged simulation. It is worth noting that only an instantaneous schlieren image is available for this condition therefore additional LES studies on this condition would be of great interest for the authors to have a more robust comparison. In addition to the ambient temperature variation, Figure 16 and 17 show the validation of the current CSE-FGM combustion model under different ambient oxygen concentration conditions. For each of these tests a new tabulated manifold was generated (a requirement of the CSE-FGM approach). The CSE-FGM model was able to accurately predict the variation of ignition delay with oxygen concentration. This is likely due to the inclusion of strain effect on the current implementation of flamlet generated manifold. The existence of a critical strain rate for autoignition has been explored in various of experiments for different fuels where autoignition is found to be closely related to the strain rate (or scalar dissipation) [23]. There is a slight overprediction on the flame lift-off length for the CSE-FGM model; however, this overprediction is within the experimental range and comparable to other approaches [18][6]. The WSR model overpredicted both ignition delay time and the lift-off length especially in the low temperature conditions. Overall the CSE-FGM approach can accurately

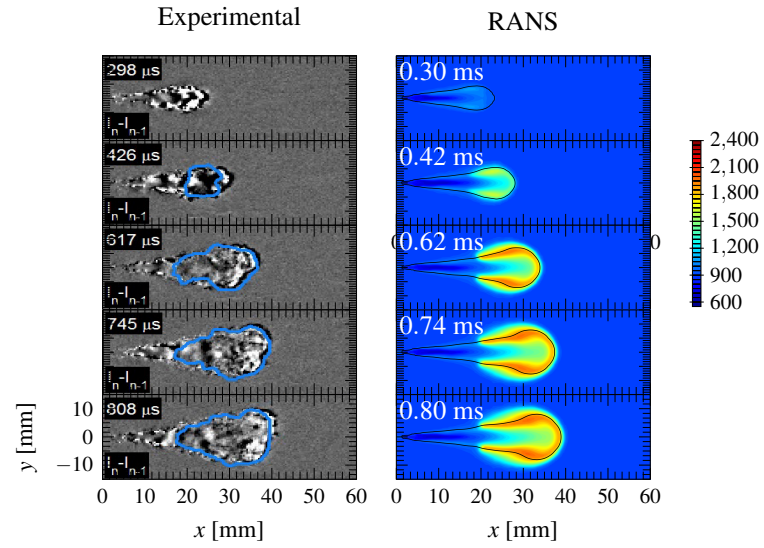


Figure 15. Schlieren image (left) and instantaneous temperature fields for CSE-FGM RANS (right) simulations at the 900K “Spray A” baseline condition. The time after start of injection is shown at the top left of image. The blue line in experimental study shows luminosity border. The black line is the stoichiometric mixture fraction contour. The experimental images are corrected by its background intensity ($I_n - I_{n-1}$).

predict the ignition delay time and flame lift-off length for a range of ambient conditions. The characteristics of autoignition and the following flame propagation is in qualitatively agreement with the experiments.

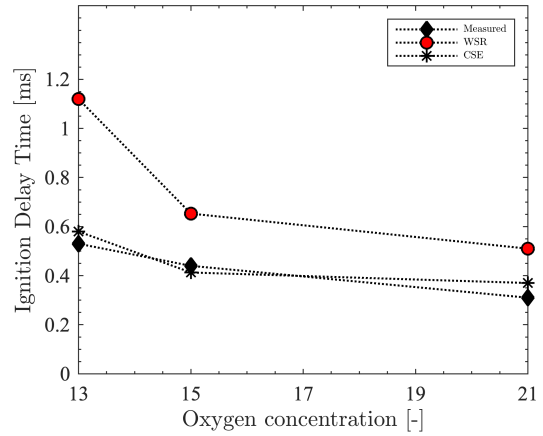


Figure 16. Simulation and experimental ignition delay timings for different “Spray A” ambient oxygen concentrations.

Combustion Recession

For the study of combustion recession, the RANS CSE-FGM simulation is continued after the start of the ramp down (ASoR = 1.4 ms after start of injection) and stopped at 2.0 ms after the start of injection. As previously noted, earlier studies by the authors have explored the effects of different combustion models, chemical mechanisms and ambient boundary conditions in predicting the existence of combustion recession. Figure 18 shows the temperature contours for the “Spray A” baseline conditions at three different times after the start of

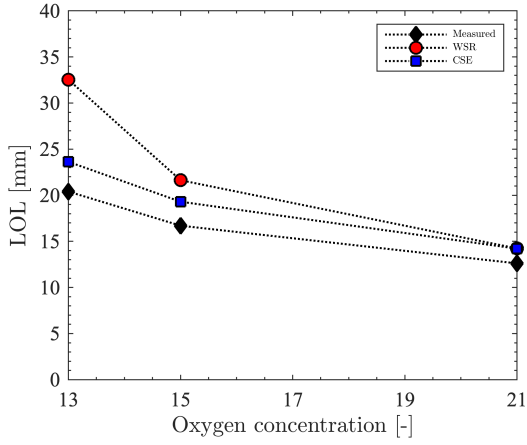


Figure 17. Simulation and experimental lift-off length for different “Spray A” ambient oxygen concentrations.

ramp down with the comparison of previous simulation results and the experimental chemiluminescence OH* images. The CSE-FGM model is compared with the WSR model, the representative iterative flamelet (RIF) model, the flamelet generated manifold combustion model (note here FGM is used as a combustion model rather than a tabulation method for chemistry) and the experimental data from Jarrahbashi *et al.* [13]. The reason for the comparison between experimental OH* and the temperature contour is due to the lack of excited state OH radical in the current chemical mechanism. Comparing simulated ground state OH with the experimental excited state OH would not be accurate as differences have been observed between these two values in experiments [22]. The OH* image from the experiment is used as a qualitative indication of high temperature contour therefore compared with the simulated temperature field. Note that the low level signal seen near the injector nozzle is likely caused by the noise and/or background reflection which should not be considered as the chemiluminescence signal from reacting mixtures. The 20 mm by 30 mm window size for this comparison is determined by the experimental window size as no other optical results are available to the authors for combustion recession. All combustion models show similar flame penetration length with the SAGE model predicting the highest temperature as expected due to the exclusion of higher order non-linear mixing in turbulent chemistry and the RIF model predicting a more diffused temperature field. Compared to other models, the FGM model produces a slight narrower span of the reaction zone with the predicted temperature being lower compared to that of the SAGE model. The narrower reaction zone can be linked to the progress variable source term being calculated using a kinetic model in this particular implementation [8]. Similar findings can be found in Kim *et al.*'s study using a traditional RANS-FGM modeling approach [14]. The CSE-FGM model shows a more physically realistic temperature profile compared to the WSR and FGM. However similarly to the RIF approach, the inclusion of turbulence chemistry interaction in CSE-FGM has prolonged the lift-off length prediction compared to an FGM combustion model approach. It can be seen from the experiment that combustion recession is started from around ASor 344 μ s where OH* is seen to start propagating back to

the nozzle with indication of separated ignition pocket. From the simulations all models have clearly shown signs of combustion recession to the injector nozzle at ASor 344 μ s. The CSE-FGM, FGM and RIF model showed a further recession back to the nozzle compared to the WSR model. For the FGM model it is shown a higher temperature is recession is given at this stage of simulation. Both the RIF and CSE-FGM, however, present a more diffused flame recession owing to their inclusion of turbulent chemistry interaction and the effect of scalar dissipation rate.

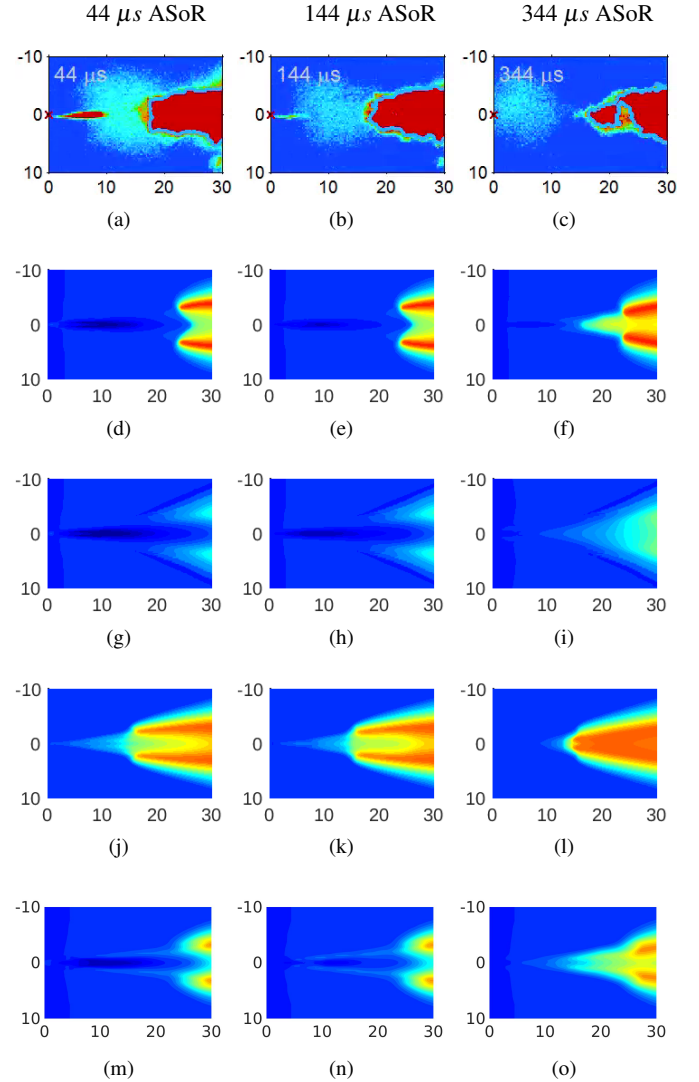


Figure 18. 900 K “Spray A” baseline conditions simulation temperature contours compared with experimental chemiluminescence OH* imaging: (a) (b) (c): Experiment [26] , (d) (e) (f): SAGE, (g) (h) (i): RIF, (j) (k) (l): FGM, (m) (n) (o): CSE-FGM. All temperature contours presented here use the same colour scheme given in Figure 15.

Following the comparison of the simulated combustion recession timing with the experiment, the differences of the predicted physical characteristics of combustion recession using different combustion models are explored. Figure 19 compares the simulated end of injection combustion recession between the WSR combustion model and the CSE-FGM model. As described before, both models predicted similar flame penetration and flame region with the WSR model giving a higher temperature profile. However the differences are found at 1.8 ms after start of injection, where a separate high

temperature ignition kernel is found in the CSE-FGM model. This can be seen as an autoignition event linked to the high entrainment wave at the end of injection causing the fluctuations of the scalar dissipation rate. Following the localized autoignition at 1.8 ms, the flame reaction zone propagates around the autoignition kernel at 1.9 ms and eventually connected to the main reaction zone. This predicted combustion recession characteristic is similar to observations from experimental studies where flame recession is recorded in the form of a series of discrete ignition pockets. In contrast, while the WSR model was able to capture a combustion recession event it is seen as flame propagation rather than separated autoignition event. The capability of the CSE-FGM combustion model to capture the autoignition characteristic of combustion recession lies in the explicit presence of the scalar dissipation in CMC type combustion models which are capable of indicating small effects of small-scale mixing on autoignition. The CSE-FGM model framework also include the conditional correlation between the fluctuations of a scalar (mixture fraction in this particular case) and the scalar dissipation rate, hence making it more appropriate to study combustion events closely correlated to scalar dissipation fluctuations. The differences between two combustion models suggest that the inclusion of the turbulent chemistry interaction, the strain effect (scalar dissipation rate) and low-temperature chemistry can be the key to accurately capturing the low temperature combustion end of injection event, combustion recession.

Conclusions

Three dimensional diesel “Spray A” simulations have been performed in this study using a newly developed combustion model, CSE-FGM, under RANS turbulence framework. This is the first time that the CSE approach has been applied to a complex/heavy hydrocarbon fuel. The objectives of this study were to: (1) validate the combustion model against the experimental data over a range of ambient conditions (2) study the flame autoignition and propagation characteristics using the new combustion model (3) apply the new model to the study of diesel spray end of injection phenomenon, combustion recession.

Non-reacting evaporating spray simulations at “Spray A” baseline conditions were validated against experimental results from the ECN database. The chosen spray sub-models showing good agreement for global parameters such as liquid and vapor penetration and also local parameters of radial mixture fraction distribution.

Reactive simulations were carried out in CONVERGE with flamelet solutions generated from CHEM1D. The CSE-FGM RANS based combustion modelling approach successfully demonstrated the capability of realistically predicting the essential structure of the diesel-fueled transient spray combustion processes. The RANS simulations are capable of quantitatively predicting the ignition delay time and flame lift-off length over a range of ambient conditions. The RANS temperature-mixture fraction scatter plot also suggested the CSE-FGM can capture the two stage ignition existed in diesel combustion. Simulations from the CSE-FGM model are also

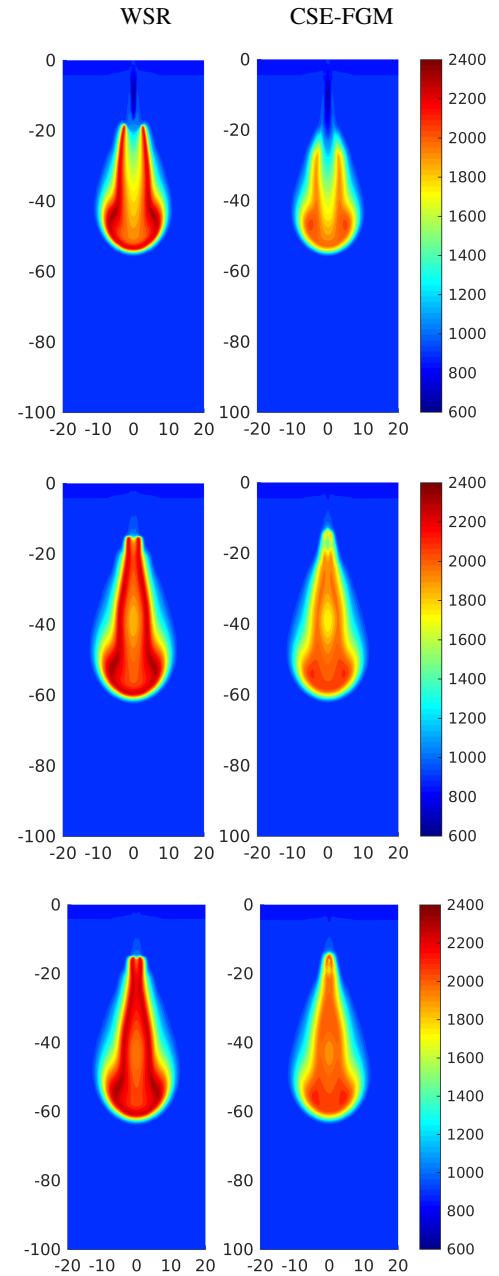


Figure 19. Temperature profiles comparison between WSR and CSE-FGM. Top, middle and bottom correspond respectively to 1.44 ms (40 μ s ASoR), 1.84 ms (440 μ s ASoR) and 1.94 ms (540 μ s ASoR) after start of injection.

compared with the WSR model. It is shown that the CSE-FGM model leads to more accurate results especially in low temperature conditions. From a combustion modelling viewpoint it can be argued that the CSE-FGM approach offers a feasible tool for detailed combustion analysis of diesel spray flames.

Finally, the capability of the CSE-FGM combustion model is further studied in the predictions of combustion recession. The results show that low-temperature chemistry is a driving force for second-stage ignition in diesel spray end-of-injection processes. The CSE-FGM combustion model along with other models accurately predicted the timing of combustion recession. Strength was seen for both the RIF and CSE-FGM model in capturing further flame penetration to the injector

nozzle. The inclusion of the turbulent chemistry interaction, the strain effect (scalar dissipation rate) and low-temperature chemistry in CSE-FGM also enabled it to predict separate ignition kernel at the end of injection. Autoignition kernel was found upstream of the lift off length followed by flame reaction zone propagates around the autoignition kernel. This prediction agrees with prior experimental observations showing combustion recession is driven by a series of auto-ignition events.

Although this study has given increased physical insights for the prediction of combustion recession using the CSE-FGM approach, there is **still** room for improvement in terms of the combustion model. Only a single ignition kernel was found for autoignition and end of injection combustion recession in the current simulation compared to multiple ignition kernels visible in the experiment. This is likely caused by the RANS ensemble averaging effect. Future work would be extending the current model to an LES framework where a more data-rich solution can be obtained providing the opportunity to explore more local and unsteady phenomenon present in a transient diesel jet.

References

- [1] W. K. Bushe and H. Steiner. Conditional moment closure for large eddy simulation of nonpremixed turbulent reacting flows. *Physics of Fluids*, 11(7):1896–1906, 1999.
- [2] R. Bilger, S. Starner, and R. Kee. On reduced mechanisms for methane-air combustion in nonpremixed flames. *Combustion and Flame*, 80(2):135 – 149, 1990.
- [3] C. Blomberg, L. Zeugin, S. Pandurangi, M. Bolla, *et al.* Modeling Split Injections of ECN Spray A Using a Conditional Moment Closure Combustion Model with RANS and LES. *SAE Int. J. Engines*, 9(4), January 2016.
- [4] D. Dovizio and C.B. Devaud. Doubly Conditional Source-term Estimation (DCSE) for the modelling of turbulent stratified V-shaped flame. *Combustion and Flame*, 172, October 2016.
- [5] D. Dovizio, J. W. Labahn, and C. B. Devaud. Doubly Conditional Source-term Estimation (DCSE) applied to a series of lifted turbulent jet flames in cold air. *Combustion and Flame*, 162(5), May 2015.
- [6] G. D. Errico, T. Lucchini, F. Contino, M. Jangi, and X.-S. Bai. Comparison of well-mixed and multiple representative interactive flamelet approaches for diesel spray combustion modelling. *Combustion Theory and Modelling*, 18(1):65–88, 2014.
- [7] X. Fang, R. Ismail, and M. Davy. A study on kinetic mechanisms of diesel fuel surrogate n-dodecane for the simulation of combustion recession. *SAE Technical Paper*, 2019-01-0202, 04, 2019.
- [8] X. Fang, R. Ismail, M. H. Davy, and J. Camm. Numerical studies of combustion recession on ECN diesel Spray A. *ASME. Internal Combustion Engine Division Fall Technical Conference*, 2018-9597.
- [9] S. S. Girimaji. Assumed β -pdf model for turbulent mixing: Validation and extension to multiple scalar mixing. *Combustion Science and Technology*, 78(4-6):177–196, 1991.
- [10] R. W. Grout, W. K. Bushe, and C. Blair. Predicting the ignition delay of turbulent methane jets using conditional source-term estimation. *Combustion Theory and Modelling*, 11(6):1009–1028, 2007.
- [11] P. C. Hansen. Numerical tools for analysis and solution of fredholm integral equations of the first kind. *Inverse Problems*, 8(6):849, 1992.
- [12] R. Issa. Solution of the implicitly discretised fluid flow equations by operator-splitting. *Journal of Computational Physics*, 62(1):40 – 65, 1986.
- [13] D. Jarrahbashi, S. Kim, and C. Genzale. Simulation of combustion recession after end-of-injection at diesel engine conditions. *Journal of Engineering for Gas Turbines and Power*, 139, 03 2017.
- [14] N. Kim, K. Jung, and Y. Kim. Multi-environment pdf modeling for n-dodecane spray combustion processes using tabulated chemistry. *Combustion and Flame*, 192:205 – 220, 2018.
- [15] S. Kim, D. Jarrahbashi, and C. Genzale. The role of turbulent-chemistry interaction in simulating end-of-injection combustion transients in diesel sprays. In *SAE Technical Paper*. SAE International, 03 2017.
- [16] B. Knox, C. Genzale, L. Pickett, and J. Garcia-Oliver. Combustion Recession after End of Injection in Diesel Sprays. *SAE Int. J. Engines* 2015-01-0797, 8(2):679–695, 2015.
- [17] B. Knox and C. L. Genzale. Scaling combustion recession after end of injection in diesel sprays. *Combustion and Flame*, 177(Supplement C):24 – 36, 2017.
- [18] P. Kundu, M. M. Ameen, and S. Som. Importance of turbulence-chemistry interactions at low temperature engine conditions. *Combustion and Flame*, 183:283 – 298, 2017.
- [19] J. W. Labahn, C. B. Devaud, T. A. Sipkens, and K. J. Daun. Inverse analysis and regularisation in conditional source-term estimation modelling. *Combustion Theory and Modelling*, 18(3):474–499, 2014.
- [20] F. Leach, R. Ismail, and M. Davy. Engine-out emissions from a modern high speed diesel engine – the importance of nozzle tip protrusion. *Applied Energy*, 226:340 – 352, 2018.
- [21] M. M. Salehi, W.K. Bushe and K. J. Daun. Application of the conditional source-term estimation model for turbulence-chemistry interactions in a premixed flame. *Combustion Theory and Modelling*, 16(2):301–320, 2012.
- [22] N. Maes, M. Meijer, N. Dam, B. Somers, H. B. Toda, G. Bruneaux, S. A. Skeen, L. M. Pickett, and J. Manin. Characterization of spray a flame structure for parametric variations in ecn constant-volume vessels using chemiluminescence and laser-induced fluorescence. *Combustion and Flame*, 174:138 – 151, 2016.
- [23] E. Mastorakos. Ignition of turbulent non-premixed flames. *Progress in Energy and Combustion Science*, 35(1):57 – 97, 2009.
- [24] Y. Pei, E. R. Hawkes, M. Bolla, S. Kook, G. M. Goldin, Y. Yang, S. B. Pope, and S. Som. An analysis of the structure of an n-dodecane spray flame using tpdf modelling. *Combustion and Flame*, 168:420 – 435, 2016.
- [25] L. M. Pickett and G. Bruneaux. Engine combustion network. combustion research facility, sandia national

laboratories, livermore, ca. See <http://www.sandia.gov/ECN>, 2018.

- [26] L. M. Pickett, C. L. Genzale, G. Bruneaux, L.-M. Malbec, L. Hermant, C. Christiansen, and J. Schramm. Comparison of diesel spray combustion in different high-temperature, high-pressure facilities. *SAE Int. J. Engines*, 2010-01-2106, 3:156–181, 10, 2010.
- [27] C. M. Rhie and W. L. Chow. Numerical study of the turbulent flow past an airfoil with trailing edge separation. *AIAA Journal*, 21:1525–1532, Nov. 1983.
- [28] G. Stahl and J. Warnatz. Numerical investigation of time-dependent properties and extinction of strained methane and propane-air flamelets. *Combustion and Flame*, 85(3-4):285–299, 1991.
- [29] A. Wehrfritz, O. Kaario, V. Vuorinen, and B. Somers. Large eddy simulation of n-dodecane spray flames using flamelet generated manifolds. *Combustion and Flame*, 167:113 – 131, 2016.
- [30] T. Yao, Y. Pei, B. Zhong, S. Som, and T. Lu. A Hybrid Mechanism for n-Dodecane Combustion with Optimized Low-Temperature Chemistry. *9th US National Combustion Meeting*, 05, 2015.

Contact Information

Leo (XiaoHang) Fang
xiaohang.fang@eng.ox.ac.uk

Acknowledgements

The authors would like to thank EPSRC, The China Oxford Scholarship Fund and The Great Britain-China Scholarship Fund for the financial support. We would also like to thank Convergent Science Inc for CFD code access and the supporting baseline conditions provided by Kim Sayop and Prof. Genzale from Georgia Institute of Technology.

Definitions/Abbreviations

AMR	Adaptive Mesh Refinement
ASOI	After Start of Injection
CDF	Counterflow Diffusion Flame
CFD	Computational Fluid Dynamics
CMC	Conditional Moment Closure
CSE	Conditional Source-term Estimation
DCMC	Doubly Conditional Moment Closure
DCSE	Doubly Conditional Source-term Estimation

EOI	End of Injection
ECN	Engine Combustion Network
FGM	Flamelet Generated Manifold Model
HR	Homogeneous Reactor
ICDF	Igniting Counterflow Diffusion Flame
IDT	Ignition Delay Time
KHRT	Kelvin-Helmholtz Raleigh-Taylor
LOL	Lift-Off Length
LTC	Low Temperature Combustion
NTC	No Time Counter Model
RANS	Reynold Averaged Navier Stokes
SOI	Start of Injection
QSS	Quasi-steady State
η	Conditioning Variable in Sample Space
c	Progress Variable
Z	Mixture Fraction